Title
Investigation of iron–ammine and amido complexes within a C 3 -symmetrical phosphinic amido tripodal ligand

Journal
Dalton Transactions, 50(32)

ISSN
1477-9226

Authors
Sun, Chen
Oswald, Victoria F
Hill, Ethan A
et al.

Publication Date
2021-08-28

DOI
10.1039/d1dt01032h

Peer reviewed

Published in final edited form as:
Dalton Trans. 2021 August 28; 50(32): 11197–11205. doi:10.1039/d1dt01032h.

Investigation of Iron–Ammine and Amido Complexes within a *C*$_3$-Symmetrical Phosphinic Amido Tripodal Ligand

Chen Sun, **Victoria F. Oswald**, **Ethan A. Hill**, **Joseph W. Ziller**, **A. S. Borovik**
Department of Chemistry, University of California-Irvine, 1102 Natural Sciences II, Irvine, CA 92697-2025, United States

Abstract

The primary and secondary coordination spheres can have large regulatory effects on the properties of metal complexes. To examine their influences on the properties of monomeric Fe complexes, the tripodal ligand containing phosphinic amido groups, *N*,*N*′,*N*″-[nitrilotris(ethane-2,1-diyl)]tris(*P*,*P*-diphenylphosphinic amido) ([poat]$^{3-}$), was used to prepare [Fe$^{II/III}$poat]$^{-/0}$ complexes. The Fe^{II} complex was four-coordinate with 4 N-atom donors comprising the primary coordination sphere. The Fe^{III} complex was six-coordinate with two additional ligands coming from coordination of O-atom donors on two of the phosphinic amido groups in [poat]$^{3-}$. In the crystalline phase, each complex was part of a cluster containing potassium ions in which K---O=P interactions served to connect two metal complexes. The [Fe$^{II/III}$poat]$^{-/0}$ complexes bound an NH_3 molecule to form trigonal bipyramidal structures that also formed three intramolecular hydrogen bonds between the ammine ligand and the O=P units of [poat]$^{3-}$. The relatively negative one-electron redox potential of −1.21 V vs. [Fe$^{III/II}$Cp$_2$]$^{+/0}$ is attributed to the phosphinic amido group of the [poat]$^{3-}$ ligand. Attempts to form the Fe^{III}–amido complex via deprotonation were not conclusive but isolation of [Fe^{III}poat(NHtol)]$^{-}$ using the *p*-toluidine anion was successful, allowing for the full characterization of this complex.

Graphical Abstract

A symmetry match was achieved between an Fe^{III} synthon with phosphinic amido group and ammonia to achieve an Fe^{III}-NH_3 complex with three intramoleculat hydrogen bonds

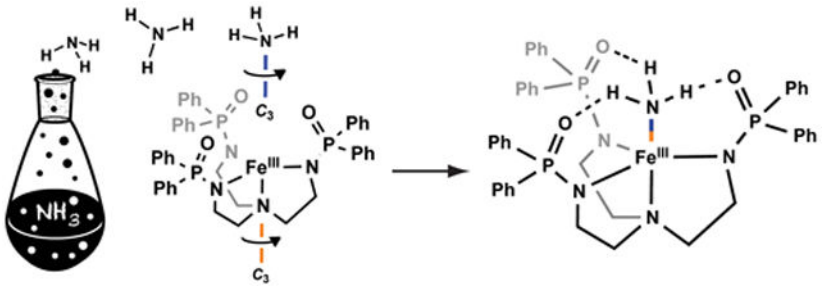

aborovik@uci.edu .

Conflicts of interest
There are no conflicts to declare

Introduction

Many of the physical and chemical properties of metal complexes are governed by the primary and secondary coordination spheres. The active sites in metalloproteins exemplify how these coordination spheres can interact to achieve highly functional systems.[1,2] One major difference between the coordination spheres is that the primary coordination sphere relies on covalent bonds whereas the secondary coordination sphere often uses non-covalent interactions, such as hydrogen bonds (H-bonds) and electrostatic interactions. There are now several examples of bioinspired synthetic complexes which were developed to better understand how the two coordination spheres cooperate.[3-7] We have been developing metal complexes with intramolecular H-bonds to investigate how these interactions affect the structure and function of first-row transition metal complexes.[8,9] Most of our studies have focused on designing tripodal ligands that have two distinct characteristics: 1) they have anionic N-atom donors within the trigonal plane to support high-valent metal centers and 2) they create relatively rigid frameworks that position H-bond donors or acceptors proximal to the metal center(s).

One symmetrical tripodal ligand that we have used is *N,N′,N″*-[2,2',2"-nitrilotris(ethane-2,1-diyl)]tris(2,4,6-trimethylbenzenesulfonamido ([MST]$^{3-}$, Figure 1A),[10,11] which provides a trianionic metal binding pocket and incorporates sulfonamido O-atoms within the secondary coordination sphere to serve as H-bond acceptors.[12,13] One limitation of using this ligand is that sulfonamido groups cannot stabilize metal centers with formal oxidation states higher than 3+.[14] To circumvent this problem, we recently introduced the related symmetrical tripodal ligand, *N,N′,N″*-[nitrilotris(ethane-2,1-diyl)]tris(*P,P*-diphenylphosphinic amido) ([poat]$^{3-}$, Figure 1C) that has phosphinic amido groups instead of sulfonamido groups, and we found that it can stabilize Fe^{IV}–oxido complexes.[15] These findings suggested that phosphinic amido donors provide a stronger ligand field than the corresponding sulfonamido groups. To provide more quantitative evidence for this difference between the properties of [MST]$^{3-}$ and [poat]$^{3-}$ (Figure 1), we have made analogous Fe complexes and directly compared the structural, vibrational, and redox properties. We chose to explore the chemistry of [$Fe^{II/III}$poat]$^{-/0}$ complexes and the related Fe—NH_3 and Fe-amido species.[16-23] The analogous Fe complexes with [MST]$^{3-}$ (Figure 1B) have been previously reported and serve as the comparison complexes.[24] Our findings clearly demonstrate that phosphinic amido groups do indeed provide a stronger ligand field that stabilize higher redox states. Moreover, our work shows that the P=O groups are excellent H-bond acceptors and assist in forming relatively strong intramolecular H-bonds.

Results and discussion

Preparations of {K[Fe^{II}poat]}$_2$ and {K[Fe^{III}poat]$_2$}$^+$

The [Fe^{II}poat]$^-$ complex was briefly mentioned in a previous report[15] and its complete preparation, properties, and molecular structure are included here. The potassium salt of the complex was prepared by treating the precursor ligand H_3poat[15] with 3 equiv of KH in THF for ~30 min and then allowing the resulting mixture to react with $Fe^{II}(OAc)_2$ which was added as a solid in one portion (Scheme 1). After filtration, {K[Fe^{II}poat]}$_2$·3THF was recrystallized by diffusing diethyl ether into a solution of the salt to obtain yellow

crystals in yields of greater than 60 %. The parallel-mode electron paramagnetic resonance (EPR) spectrum of $[Fe^{II}poat]^-$ had a signal with a g-value of 9.2 and the complex has an μ_{eff} = 4.06 μ_B, both of which are indicative of an S = 2 spin ground state (Figure S1). The electrochemical properties of $[Fe^{II}poat]^-$ were evaluated using cyclic voltammetry in THF to reveal a reversible event with an $E_{1/2}$ = −1.09 V versus $[Fe^{III/II}Cp_2]^{+/0}$ that is assigned to the $[Fe^{III/II}poat]^{0/-}$ redox couple (Figure S2). Based on this result, we chemically prepared $[Fe^{III}poat]$ by treating a suspension of $\{K[Fe^{II}poat]\}_2$ in THF with $[Fe^{III}Cp_2]BF_4$ in acetonitrile (MeCN). A homogenous solution was initially formed that slowly produced a red precipitate in 80 % yield. Isolation of $\{K[Fe^{III}poat]_2\}[BF_4]$ as a red crystalline solid was achieved after recrystallization from vapor diffusion of diether ether into an MeCN solution of the complex (Scheme 1). The EPR spectrum of this complex has g-values at 3.27, 5.52, and 7.01 and an μ_{eff} = 5.56 μ_B that are characteristic of an S = 5/2 spin ground state (Figure S3).

Structural Properties of $\{K[Fe^{II}poat]\}_2$·3THF and $\{K[Fe^{III}poat]_2\}[BF_4]$

The molecular structures of $\{K[Fe^{II}poat]\}_2$·3THF and $\{K[Fe^{III}poat]_2\}[BF_4]$ were investigated using X-ray diffraction (XRD) methods. In the crystalline phase, $[Fe^{II}poat]^-$ is part of a cluster with the formula $\{K[Fe^{II}poat]\}_2$·3THF (Figure 2A, Table 1), which crystallized in the $R\bar{3}c$ space group. Each Fe^{II} center in the $[Fe^{II}poat]^-$ complex is four-coordinate with trigonal monopyramidal coordination geometry (Figure 2B). The Fe1—N1 and Fel—N2 bond lengths are 2.127(4) and 1.994(2) Å, and the N1—Fe1—N2 angle is 83.62(7)°. The Fe center is displaced 0.222 Å from the plane formed by the deprotonated phosphinic nitrogen atoms – this displacement is toward the vacant axial coordination site. These metrical parameters are comparable to those reported for similar Fe complexes with trigonal monopyramidal geometries.[25-28] For instance, $[Fe^{II}1^{iPr}]^-$ (where $[1^{iPr}]^{3-}$ is tris-(*N*-isopropylcarbamoylmethyl)amido) has Fe1—N1 and avg. Fe—$N_{equatorial}$ bond lengths of 2.098(3) and 2.020(5) Å with the Fe center displaced 0.232 Å above the trigonal plane.[26] The structural studies also showed that the two $[Fe^{II}poat]^-$ complexes are linked through a network of potassium ions and THF molecules (Figure 2A). Each potassium ion is coordinated to an $[Fe^{II}poat]^-$ through the P=O units of the phosphinic amido groups with a K1---O1 distance of 2.651(2) Å. Each half of the cluster is linked through the three THF molecules that bridge between the two potassium ions with a K1---$O2_{THF}$ bond length of 2.750(2) Å.

For the structure of $\{K[Fe^{III}poat]_2\}[BF_4]$, our analysis gave poor quality fits to the data because of disorder problems in the phenyl rings and tren backbone of the $[poat]^{3-}$ ligand and solvent molecules within the lattice. While caution needs to be taken when describing this structure of $\{K[Fe^{III}poat]_2\}[BF_4]$, we will qualitatively discuss its structure because the metrical parameters involving the Fe1 center have acceptable esd's values. The structure also revealed a $\{K[Fe^{III}poat]_2\}^+$ cluster with the two $[Fe^{III}poat]$ complexes now linked through a single potassium ion that coordinates to the P=O units with the avg. K---O bond distances of 2.621(1) Å (Figure 3A). The cluster has an overall positive charge which within the crystal lattice is balanced by a $[BF_4]^-$ anion. Even though there is no external ligand coordinated to the Fe^{III} centers, each $[Fe^{III}poat]$ within the cluster is six-coordinate because the P=O units containing O2 and O3 are canted in a manner to form Fe1—O2 and Fe4—O3 bonds

with distance of 2.235(5) and 2.323(4) Å (Figure 3B). The remaining coordinate sites on the Fe^{III} center are the N-atoms of the $[poat]^{3-}$ with Fe1—N1 and average Fe1—$N_{equatorial}$ bond distances of 2.336(5) and 2.079(5) Å.

Synthesis and Properties of $[Fe^{II}poat(NH_3)]^-$

The vacant axial coordination site in $[Fe^{II}poat]^-$ provided an opportunity to examine the effects of binding external ligands and, as discussed above, we prepared $[Fe^{II}poat(NH_3)]^-$. Initial attempts to synthesize $K[Fe^{II}poat(NH_3)]$ from $\{K[Fe^{II}poat]\}_2 \cdot 3THF$ and NH_3 solution in THF were unsuccessful and appeared to only produce the starting $\{K[Fe^{II}poat]\}_2 \cdot 3THF$ complex. We reasoned that the strong P=O---K interactions could possibly interfere with the stability of the complex by hindering the intramolecular H-bonds that are presumably formed between the ammine ligand and $[poat]^{3-}$. To overcome this synthetic problem, we introduced [2.2.2]-cryptand (crypt) to the reaction mixture to encapsulate the K^+ ion and avoid any interactions with $[Fe^{II}poat(NH_3)]^-$. This route proved successful and the desired salt, $[K(crypt)][Fe^{II}poat(NH_3)]$ was prepared in greater than 85% yield as yellow crystals (Scheme 2). The complex has an μ_{eff} = 5.17 μ_B and a valley shaped EPR signal at g = 9.1 that are consistent with a high spin Fe^{II} center (Figure S1).

The expected molecular structure of $[K(crypt)][Fe^{II}poat(NH_3)]$ is supported by a structural analysis using XRD methods (Figure 4A). The $[Fe^{II}poat(NH_3)]^-$ has a trigonal bipyramidal primary coordination geometry in which $[poat]^{3-}$ ligand binds in the same way as observed in $[Fe^{II}poat]^-$ (Tables 1 and 2) The N-atoms of the phosphinic amido groups define the trigonal plane with an avg. Fe1—$N_{equatorial}$ bond length of 2.108(2) Å. The external ammine ligand is bound to an axial site with an Fe1—N5 bond length of 2.143(2) Å and is trans to the apical N-atom of $[poat]^{3-}$. The Fe1—N1 bond length of 2.220(1) Å in $[Fe^{II}poat(NH_3)]^-$ is significantly longer than that found in $[Fe^{II}poat]^-$ which is attributed to the trans influence from coordination of NH_3. A commensurate increase of 0.144 Å was observed for the displacement of the Fe^{II} center from the trigonal plane toward the ammine ligand in $[Fe^{II}poat(NH_3)]^-$. The potassium ion is encapsulated by the crypt with an avg. K---O distance of 2.825(3) Å and is not interacting with $[Fe^{II}poat(NH_3)]^-$.

The $[poat]^{3-}$ ligand was designed to support intramolecular H-bonds and the molecular structure of $[Fe^{II}poat(NH_3)]^-$ demonstrates that this type of non-covalent interaction is possible within the secondary coordination sphere of the Fe center. Three intramolecular H-bonds are present that are formed between the ammine ligand and phosphinic amido groups of $[poat]^{3-}$ (Table 2). As found in $[Fe^{II}MST(NH_3)]^-$, there is a match between the symmetries of the $[poat]^{3-}$ ligand with that of the NH_3 ligand to align the N—H groups to form H-bonds with the O-atoms of phosphinic groups. We note that the overall molecular structures of $[Fe^{II}poat(NH_3)]^-$ and $[Fe^{II}MST(NH_3)]^-$ are nearly equivalent with the same arrangement of N-atom donors within the primary coordination sphere and the number of H-bonds within secondary coordination sphere. However, the sodium ion interactions in $Na[Fe^{II}MST(NH_3)]$ prevent a direct comparison between the two complexes.

Electrochemical Properties of $[Fe^{II}poat(NH_3)]^-$

The CV of $[Fe^{II}poat(NH_3)]^-$ measured in DCM:THF revealed a one-electron reversible redox couple at $E_{1/2}$ = −1.21 V (Figure 5). This potential is 0.57 V more negative than the analogous redox process found in $[Fe^{II}MST(NH_3)]^-$ which has an $E_{1/2}$ = −0.64 V versus $[Fe^{III/II}Cp_2]^{+/0}$ in DCM:THF (Figure S4). This large difference in redox potentials agrees with our other observations that phosphinic amido groups are useful in stabilizing higher oxidized metal complexes. For example, we recently showed that $[poat]^{3-}$ can stabilize an unusual high-spin Fe^{IV}=O complex which is not possible with tripodal sulfonamido ligands.[14,15] Because the structures of $[Fe^{II}poat(NH_3)]^-$ and $[Fe^{II}MST(NH_3)]^-$ are the same (Figure 4B, ref 24) we suggest that a key contributor to the difference in their redox potentials is that the phosphinic amido donors are stronger σ-donors to the Fe center than sulfonamido groups.

Preparation and Structure of $[Fe^{III}poat(NH_3)]$

We again used the information obtained from the CV experiments and chose $[Fe^{III}Cp_2]BF_4$ to prepare the one-electron oxidized analogue of K(crypt)$[Fe^{II}poat(NH_3)]$. Two independent routes were used (Scheme 2): a direct oxidation of K(crypt)$[Fe^{II}poat(NH_3)]$ in THF/MeCN and an indirect method that first treated solid $\{K[Fe^{II}poat]\}_2$ with THF solution of NH_3 which was followed by oxidation with $[Fe^{III}Cp_2]BF_4$. Both routes afforded the neutral species $[Fe^{III}poat(NH_3)]$ in similar yields and purity. We also examined treating $\{K[Fe^{III}poat]_2\}[BF_4]$ directly with NH_3 to produce $[Fe^{III}poat(NH_3)]$, but the purity and yields were significantly poorer than the other routes and was not further studied. The absorption spectrum of $[Fe^{III}poat(NH_3)]$ is dominated by a strong band at λ_{max} (ε_M) = 380 nm (4260 $M^{-1}cm^{-1}$, Figure 6A) and a shoulder at 510 nm. An axial EPR spectrum was observed for $[Fe^{III}poat(NH_3)]$ with g-values at ~6 and 2 that suggests an S = 5/2 spin system with C_3 symmetry in solution (Figure 6B). Consistent with this finding is a measured μ_{eff} of 5.88 μ_B.

The molecular structure of $[Fe^{III}poat(NH_3)]$ was determined by XRD methods to show a similar trigonal bipyramidal coordination as discussed for $[Fe^{II}poat(NH_3)]^-$. $[Fe^{III}poat(NH_3)]$ crystalized in the $P\bar{3}$ space group with the NH_3 ligand being on a principle C_3-rotational axis with respect to the Fe—N5 bond; in addition, there are two crystallographically different, but chemically equivalent, molecules in the asymmetric unit and we will discuss the average of their metrical parameters (Figures 4B & S5, Table 2). The Fe—N2 and Fe—N5 bond distances of 1.998(2) and 2.051(1) Å in $[Fe^{III}poat(NH_3)]$ are significantly shorter than those found in its Fe^{II}—NH_3 analogue which is consistent with oxidation of the Fe center. Moreover, $[Fe^{III}poat(NH_3)]$ is a neutral species which lacks a coordinated potassium ion as was found in the structure of $\{K[Fe^{III}poat]_2\}[BF_4]$.

The similar structures of the neutral $[Fe^{III}poat(NH_3)]$ and $[Fe^{III}MST(NH_3)]$ complexes offer a direct comparison on the structural effects of these two tripodal ligands. There is a small, but statistically significant decrease in the Fe—N5 bond length in $[Fe^{III}poat(NH_3)]$ compared to that in $[Fe^{III}MST(NH_3)]$ (2.060(4) versus 2.080(3) Å) but a larger decrease in the Fe—N1 bond distance (2.220(4) versus 2.295(3) Å). In addition, there is an over 0.1 Å increase in the N5…O1 distances from $[Fe^{III}poat(NH_3)]$ (2.774(3) Å) to $[Fe^{III}MST(NH_3)]$

(2.881(2) Å). These heavy atom distances are used as a marker to gauge the strength of a H-bond and suggest that stronger intramolecular H-bonds are formed in [Fe^{III}poat(NH_3)]. The stronger N5—H1…O1 in [Fe^{III}poat(NH_3)] is attributed to the combination of two effects: 1) the stronger Fe—N5 interaction in [Fe^{III}poat(NH_3)] should increase the acidity of the ammine ligand which should make it a better H-bond donor and 2) the stronger dipole in the P=O units of the phosphinic amido group should make it a better H-bond acceptor than the S=O units in the sulfonamido ligand. In addition, for [Fe^{III}poat(NH_3)] we were able to locate the hydrogen atoms on the ammine ligand to give N—H and H…O distances of 0.84(3) Å and 1.98(3) Å that further support the presence of intramolecular H-bonds. Unfortunately, the analogous H-atoms in [Fe^{III}MST(NH_3)] could not be located in the difference map for comparison.

The structural differences between [Fe^{III}poat(NH_3)] and [Fe^{III}MST(NH_3)] are supported by solid state vibrational studies using Fourier transform infrared (FT-IR) spectroscopy (Figure 7). For [Fe^{III}poat(NH_3)], the energies of N—H vibrations of the ammine ligand were observed at 3183 and 3109 cm^{-1} while those in [Fe^{III}MST(NH_3)] were found at 3339 and 3309 cm^{-1}. The significantly lower values in [Fe^{III}poat(NH_3)] are consistent with weakening of the N—H bond that would arise from a stronger H-bond involving $[poat]^{3-}$. For comparison, there were no observable vibrational features above 3100 cm^{-1} for {K[Fe^{II}poat]}$_2$ and {K[Fe^{III}poat]$_2$}(BF_4).

Investigation of Fe^{III}–amido Complexes

The coordination of NH_3 to the Lewis acidic Fe^{III} center in [Fe^{III}poat(NH_3)] suggests that we may be able to deprotonate the ammine ligand to prepare the corresponding Fe^{III}—amido complex. We screened a series of non-coordinating bases to attempt this deprotonation and the reactions were monitored using UV-vis and EPR spectroscopies. For instance, addition of 1,8-diazabicyclo[5.4.0]undec-7-ene (DBU, p$K_{a,THF}$ =16.8) to [Fe^{III}poat(NH_3)] resulted in only small changes in the optical and axial EPR spectra that indicated that the pK_a of Fe^{III}—NH_3 unit was higher than 16.8 (Figure S6). A reaction was observed when the stronger base 1,5,7-triazobicyclo[4.4.0]dec-5-ene (TBD, p$K_{a,THF}$ = 21.0) was used and the new species had an absorption band at λ_{max} = 335 nm (Figure 6A). In addition, there was a pronounced change in the EPR properties after deprotonation from the axial EPR spectrum of [Fe^{III}poat(NH_3)] to a rhombic S = 5/2 spectrum with g-values at 9.33, 4.80, and 3.88 (Figure 6B). This new spectrum is consistent with the formation of a putative $[Fe^{III}poat(NH_2)]^-$ species in which the rhombicity would increase because it is no longer C_3-symmetric. Several attempts to grow single crystals of this deprotonated product to understand its molecular structure were unfortunately unsuccessful.

To further explore the binding of exogenous amido ligand to [Fe^{III}poat], we prepared the new Fe^{III}—NHtol complex, where NHtol is the *p*-toluidine anion. The formation of Fe^{III}—N(H)R complexes are known and nearly all are prepared from the treatment of $Fe^{II/I}$ complexes with organic azides or N-group transfer reagents.[29-38] The synthesis of $[Fe^{III}poat(NHtol)]^-$ relied on the deprotonation of *p*-toluidine with KH prior to addition to a suspension of $\{K[Fe^{III}poat]_2\}^+$,(Scheme 3). The reaction mixture immediately changed from orange to dark green which is consistent with formation of an Fe^{III}—NHtol specie.

For example, the absorption spectrum (Figure 8A) of $[Fe^{III}poat(NHtol)]^{-}$ contains bands at λ_{max} (ε_M) = 344 (5210) and 672 (2040) nm that are similar to those observed in the related $[Fe^{III}H_21(NHtol)]^{-}$ complex (λ_{max} (ε_M) = 410 (4000), 582 (2000), where $[H_21]^{3-}$is bis[(*N*-*tert*-butylureayl)-*N*-ethyl]-(*N*″-isopropylcarbamoyl-methyl)aminato.[33] In addition, the EPR spectrum of $[Fe^{III}poat(NHtol)]^{-}$ contains signals at g-values at 8.8, 5.2, and 3.5 that are also similar to $[Fe^{III}H_21(NHtol)]^{-}$ and consistent with a rhombic Fe^{III} complex with S = 5/2 spin ground state (Figure 8B).

The structure of the $K[Fe^{III}poat(NHtol)]$ also aggregated in the crystalline phase (Figure S7) with two $[Fe^{III}poat(NHtol)]^{-}$ complexes interacting with two potassium ions. The molecular structure of just the $[Fe^{III}poat(NHtol)]^{-}$ complex supports our findings in solution of an Fe^{III}—amido complex (Figure 9) with a trigonal bipyramidal geometry similar to that observed for $[Fe^{III}poat(NH_3)]$. The external amide ligand is bound to the axial position of the Fe^{III} center with an Fe1—N5 bond length of 1.950(3) Å. The Fe1—N1 and avg. Fe1—$N_{equitorial}$ bond length are 2.401(3) and 2.025(5) Å. The Fe center is displaced 0.454 Å from the plane formed by the deprotonated phosphinic nitrogen atoms which is a significant increase from that found in $[Fe^{III}poat(NH_3)]$. Similar metrical parameters were found when $[Fe^{III}poat(NHtol)]^{-}$ was compared to the structure of $K[Fe^{III}H_21(NHtol)]$, except that the Fe1—N1 bond length is significantly longer (0.210 Å) with the $[poat]^{3-}$ ligand. However, a major structural difference was found between the secondary coordination spheres in $K[Fe^{III}poat(NHtol)]$ and $K[Fe^{III}H_21(NHtol)]$. Unlike $K[Fe^{III}H_21(NHtol)]$, there are no H-bond donors in the $[poat]^{3-}$ framework and thus there are no interoactions with the N5. Furthermore, the O-atoms on P=O groups interact with the potassium ions and do not serve as H-bond acceptors to the amido N—H bond. However, there is another type of non-covalent interaction: π-π stacking interactions were observed between the aromatic rings on the $[NHtol]^{-}$ ligand and one of the phosphinic amido groups with a centroid-to-centroid distance of 3.617 Å.

Conclusions

Tripodal ligands offer a convenient way to design metal complexes in which control of both the primary and secondary coordination spheres can be achieved. These features are illustrated in the $Fe^{II/III}$ chemistry with the tripodal $[poat]^{3-}$ in which the three phosphinic amido groups provide a strong ligand field *and* control the secondary coordination sphere through the appended P=O groups. Our structural work on the $[Fe^{II/III}poat]^{-/0}$ complexes further illustrate this ligand's versatility: $[poat]^{3-}$ is a tetradentate ligand in the Fe^{II} complex with a trigonal monopyramidal coordination geometry that is derived from the tripod's N_4 donor set. In the Fe^{III} analogue, $[poat]^{3-}$ is a hexadentate ligand with two additional O-atom donors being provided by P=O units of the phosphinic amido groups. These additional donors are presumably needed to help stabilize the increased positive charge at the metal center. In addition, the structures show the propensity of the P=O unit to bind additional metal ions that results in clusters within the crystal lattices. This ability is highlighted by the cluster formed with the neutral Fe^{III} complex whereby two $[Fe^{III}poat]$ molecules are linked by a single potassium ion to form $\{K[Fe^{III}poat]_2\}BF_4$.

Experiments aimed at binding an external ligand showed the important role of non-covalent interactions within the secondary coordination on the stability of metal complexes. Attempts to coordinate ammonia to $\{K[Fe^{II}poat]\}_2$ were unsuccessful and analysis of isolated solids indicated that no binding had occurred. One possibility is that the interactions of the potassium ion with $[Fe^{II}poat]^-$ limited access to the Fe^{II} center which hindered the binding of ammonia. We found that isolating the potassium ion within a cryptand alleviated these interactions and allowed formation of $[Fe^{II}poat(NH_3)]^-$ which has a molecular structure that shows a trigonal bipyramidal coordination geometry. The structure also established the presence of three intramolecular H-bonds between the NH groups for the ammine ligand and the P=O groups of the phosphinic amido groups, which was corroborated by results from FT-IR studies. The low one-electron redox potential for Fe^{II}—NH_3 complex allowed for isolation and characterization of $[Fe^{III}poat(NH_3)]$ which also contains three intramolecular H-bonds. A similar H-bond network was found in $[Fe^{III}MST(NH_3)]$ that used a tripodal ligand with sulfonamido groups that led to structural and electrochemical comparisons between the two neutral Fe^{III}—NH_3 complexes. Our findings indicated that $[poat]^{3-}$ is better at stabilizing higher oxidized metal centers that we suggest is because the phosphinic amido groups provide a stronger ligand field *and* form stronger H-bonds.

Attempts to convert $[Fe^{III}poat(NH_3)]$ to the mono-deprotonated ion $[Fe^{III}poat(NH_2)]^-$ yielded a relatively unstable species with a structure that could not be determined. We therefore prepared the amido complex $[Fe^{III}poat(NHtol)]$ which was synthesized by a straightforward route from $\{K[Fe^{III}poat]_2\}[BF_4]$ and deprotonated *p*-toluidine. The molecular structure illustrates the formation of the five-coordinate amido complex which is supported by spectroscopic data. Taken together, our studies illustrate the versatility of the $[poat]^{3-}$ ligand in the preparation of metal complexes; more generally, these results show the utility of incorporating phosphinic amido groups in the design of new ligands.

Experimental

General Procedures

Unless otherwise stated, all reactions were performed under an argon atmosphere in a Vac Nexus One dry box. Solvents were sparged with argon and dried over columns containing Q-5 and molecular sieves. $Fe^{II}(OAc)_2$[39] and $[Fe^{III}Cp_2]BF_4$[40] were synthesized following literature procedures and stored under Ar atmosphere at room temperature. Potassium hydride as a 30% suspension in mineral oil was filtered with a medium pore size glass fritted funnel and washed with 10 mL pentane and 10 mL Et_2O five times or until the powder is white, then dried under vacuum and stored under Ar atmosphere at room temperature. NH_3 was purchased from Sigma-Aldrich as 0.4 M THF solution and used without further purification. [2.2.2]-cryptand was purchased from Sigma-Aldrich and dried under vacuum with gentle heat (40-50 °C) for more than 24 hours and stored under Ar atmosphere at room temperature. 1,5,7-triazobicyclo[4.4.0]dec-5-ene and p-toluidine was purchased from Sigma-Aldrich and used without further purification. *N,N′,N″*-(nitrilotris(ethane-2,1-diyl))tris(P,P-diphenylphosphinicamide) (H_3poat), $\{K[Fe^{II}poat]\}_2$, and $Na[Fe^{II}MST(NH_3)]$ were synthesized following our established procedures.[15,24]

Physical Methods

All electronic absorption spectra were collected in a 1 cm quartz cuvette with a magnetic spin bar inside. Room temperature electronic absorption spectra for determining extinction coefficients were recorded on a Cary 50 spectrometer. Temperature controlled time dependent electronic absorption spectra were recorded either on a Cary 60 spectrometer equipped with Quantum Northwest TC1 temperature controller and stirrer, or on an 8453E Agilent UV-vis spectrometer equipped with an Unisoku Unispeks cryostat. Cyclic voltammetry was performed using a CHI600C electrochemical analyzer under Ar atmosphere with 0.1 M tetrabutylammonium hexafluorophosphate as the supporting electrolyte. A 2.0 mm glassy carbon electrode was used as working electrode; a Pt wire was used as counter electrode; a Ag wire was used as references electrode with ferrocenium/ferrocene($FeCp_2^{+/0}$) couple as internal standard. All potentials are referenced to $FeCp_2^{+/0}$ couple. Solid-state IR spectra were collected on a Thermo Scientific Nicolet iS5 FT-IR spectrometer equipped with an iD5 ATR accessory. X-band EPR spectra were recorded as frozen solutions using a Bruker EMX spectrometer equipped with an ER041XG microwave bridge, an Oxford Instrument liquid-helium quartz cryostat, and a dual-mode cavity (ER4116DM). Magnetic moments were done by Evans's method at 298 K in CH_2Cl_2 on a Bruker DRX NMR spectrometer.[41]

Synthesis of $\{K[Fe^{II}poat]\}_2$ [15]

To a clear colorless solution of H_3poat (0.200 g, 0.268 mmol) in 4 mL THF, KH (33.4 mg, 0.833 mmol) was added and stirred for 30 minutes until gas evolution ceased. $Fe(OAc)_2$ (47.8 mg, 0.275 mmol) was added to the reaction mixture, resulting in immediate change to yellow heterogeneous solution. After stirring for 20 minutes, insoluble salt (KOAc) was filtered off through a medium pore size frit, and the resulting clear yellow solution was layered under Et_2O. Yellow x-ray quality crystals were obtained on the following day (217.2 mg, 96.5%). Note that the reaction time of this experiment is crucial for a good yield due to solubility of the product. Elemental analysis calcd for $C_{42}H_{42}FeKN_4O_3P_3$: C, 60.15; H, 5.05; N, 6.7%, found: C, 60.2; H, 4.91; N, 6.7%. FT-IR (diamond ATR, cm^{-1}): 3066, 3045, 3004, 2952, 2896, 2831, 2805, 1977, 1890, 1824, 1774, 1673, 1612, 1589, 1571, 1482, 1462, 1443, 1432, 1364, 1346, 1334, 1292, 1271, 1264, 1234, 1181, 1153, 1136, 1130, 1115, 1101, 1066, 1041, 1027, 1020, 998, 966, 951, 919, 910, 852, 802, 785, 746, 716, 695, 619, 578, 571, 569, 561, 554. EPR (X-band, //-mode, 1:1 DMF:THF, 10K): g = 9.10. μ_{eff} = 4.06 μ_B.

Synthesis of $\{K[Fe^{III}poat]_2\}[BF_4]$

$\{K[Fe^{II}poat]\}_2$ (0.446 g, 0.532 mmol) was suspended in 4 mL THF. In a separate vial, $FcBF_4$ (0.146 g, 0.536 mmol) was dissolved in 0.5 mL MeCN and added to the suspension to yield an immediate color change to clear red solution. As the reaction was stirred for 2 hours, orange precipitate formed over time. The orange solid was collected through a medium pore size frit and dried under vacuum (0.393 g, 92.3%). Crystals can be obtained by redissolving the complex in MeCN and layering under Et_2O, or by redissolving the complex in DCM and layering under pentane. Elemental analysis calcd for $C_{42}H_{42}FeN_4O_3P_3{\cdot}2KBF_4$: C, 48.0; H, 4.0; N, 5.3%, found: C, 47.90; H, 4.0; N, 5.3%. FT-IR (diamond ATR, cm^{-1}):

3073, 3052, 2961, 2893, 2853, 1977, 1897, 1821, 1779, 1676, 1615, 1591, 1571, 1483, 1447, 1435, 1306, 1278, 1194, 1180, 1121, 1090, 1050, 1034, 1025, 996, 979, 958, 950, 913, 618, 591, 589, 583, 574, 569, 565, 558, 556. EPR (X-band, ⊥-mode, MeCN, 77K): g = 7.01, 5.52, 3.27 1.90. μ_{eff} = 5.56 μ_B. UV-vis λ_{max}(MeCN)/nm (ε, $M^{-1}cm^{-1}$): 335(4900), 385(5800).

Synthesis of K(crypt)[Fe^{II}poat(NH_3)]

To $\{K[Fe^{II}poat]\}_2$ (0.462 g, 0.551 mmol), 11 mL (excess) of 0.4 M NH_3 in THF was added via syringe and stirred for 5 minutes, resulting a clear intense yellow solution. After all crystals were dissolved, [2.2.2]-cryptand (0.219 g, 0.582 mmol) was added to slowly precipitate yellow solid product. The solid was collected through a medium pore size frit, washed with 2 mL THF, dried under vacuum, redissolved in DCM, and layer under pentane. Dark yellow polygon shaped x-ray quality crystals (0.616 g, 90.7 %) were obtained the following day. Elemental analysis calcd for $C_{60}H_{81}FeKN_7O_9P_3$·2DCM: C, 53.1; H, 6.1; N, 7.0%, found: C, 53.1; H, 6.2; N, 6.8%. FT-IR (diamond ATR, cm^{-1}): 3310 (NH), 3066, 3002, 2965, 2952, 2871, 2820, 2801, 1980, 1909, 1821, 1811, 1774, 1674, 1635, 1614, 1589, 1572, 1490, 1480, 1474, 1458, 1445, 1431, 1363, 1353, 1301, 1286, 1276, 1258, 1241, 1235, 1226, 1180, 1166, 1151, 1111, 1097, 1084, 1066, 1049, 998, 971, 945, 934, 851, 833, 812, 746, 730, 721, 715, 703, 696, 618, 602, 594, 584, 578, 573, 569, 563, 557, 554. EPR (X-band, //-mode, 1:1 DMF:THF, 10K): g = 9.11. μ_{eff} = 5.17 μ_B.

Synthesis of [Fe^{III}poat(NH_3)]

K(crypt)[Fe^{II}poat(NH_3)] (0.201 g, 0.163 mmol) was suspended in 4 mL THF. In a separate vial, $FcBF_4$ (45.3 mg, 0.166 mmol) was dissolved in 0.5 mL MeCN and added to the suspension, resulting in immediate color change to red and clear solution. As the reaction was stirred for 2 hours, red precipitate formed over time. 10 drops of Et_2O were added and stirred for an additional hour to help precipitate more of the red solid product. The red solid was collected through a medium pore size frit, washed with 2 mL THF, 10 mL pentane, and 10 mL Et_2O, then dried under vacuum (99.6 mg, 74.7 %). Red needle shaped x-ray quality crystals were obtained by redissolving the red solid in DCM and layering under pentane. Elemental analysis calcd for $C_{42}H_{45}FeN_5O_3P_3$·2.5DCM: C, 51.95; H, 4.9; N, 6.8%, found: C, 52.4; H, 4.8; N, 7.0%. FT-IR (diamond ATR, cm^{-1}): 3182 (NH), 3072 (NH), 3108, 3050, 2977, 2910, 2890, 2858, 2848, 1980, 1900, 1830, 1819, 1783, 1688, 1671, 1617, 1590, 1572, 1482, 1471, 1465, 1446, 1441, 1434, 1356, 1347, 1313, 1307, 1289, 1273, 1232, 1182, 1172, 1157, 1146, 1118, 1107, 1101, 1067, 1028, 998, 995, 964, 932, 882, 849, 824, 801, 763, 757, 747, 720, 700, 696, 620, 614, 587, 577, 568, 562, 559 ,553. EPR (X-band, ⊥-mode, 1:1 DCM:THF, 77K): g = 5.58, 2.00. μ_{eff} = 5.88 μ_B. UV-vis λ_{max}(DCM)/nm (ε, $M^{-1}cm^{-1}$): 382(4300), 513(sh).

Synthesis of K[Fe^{III}poat(NHtol)]

p-toluidine (13.7 mg, 0.128 mmol) was dissolved in 2 mL THF and KH (5.4 mg, 0.13 mmol) was added to the solution, resulting in immediate formation of bubble. After stirring for an hour or until all bubble ease, the pale yellow reaction solution was filtered and added into orange solid of $\{K[Fe^{III}poat]_2\}[BF_4]$ (0.100 g, 0.125 mmol), resulting in immediate color change to a dark green solution. After stirring for two hours, the reaction solution

was dried under vacuum to obtain green solid product (0.111 g, 94.1%). X-ray quality crystals were obtained by redissolving the green solid in DCM and layering under pentane. Elemental analysis calcd for $C_{49}H_{50}FeKN_5O_3P_3$-DCM: C, 58.3; H, 5.1; N, 6.8%, found: C, 58.0; H, 4.8; N, 6.6%. FT-IR (diamond ATR, cm^{-1}): 3049 (NH), 2841, 1603, 1516, 1500, 1481, 1435, 1284, 1171, 1114, 1065, 1026, 958, 819, 793, 748, 717, 694. EPR (X-band, ⊥-mode, 1:2 DMF:THF, 3.9K): g = 8.82,5.20, 3.47. UV-vis λ_{max}(DCM)/nm (ε, $M^{-1}cm^{-1}$): 363(5210), 672(2040).

Deprotonation of [Fe^{III}poat(NH_3)]

Triazabicyclodecene(TBD, pK_a = 21 in THF) was used as base to deprotonate the complex. To monitor the absorption feature changes during the deprotonation process, a ~0.2 mM stock solution of [Fe^{III}poat(NH_3)] was prepared in DCM. 3 mL of above complex solution was transferred into a 1 cm pathlength cuvette with stir bar using syringe. The cuvette was sealed with a rubber septum and brought outside the glovebox to spectrometer. Stock solution of TBD was prepared with concentration of ~75 mM. 100 μL of base stock solution (10 equiv.) was injected using a 250 μL airtight locking syringe with constant stirring.

To monitor the EPR signal changes during the deprotonation process, a ~10 mM stock solution of [Fe^{III}poat(NH_3)] was prepared in DCM:THF. Two samples for comparing before and after addition of base were prepared using the same complex stock solution. First, 250 μL of complex stock solution was transferred into an EPR tube using syringe. The tube was sealed with a rubber septum and brought outside the glovebox to spectrometer. Second, 600 μL of complex stock solution was added into 10 equivalents of TBD solid and stirred for 1 hour. 250 μL of reaction solution was transferred into an EPR tube using syringe. The tube was sealed with a rubber septum and brought outside the glovebox to spectrometer.

Supplementary Material

Refer to Web version on PubMed Central for supplementary material.

Acknowledgements

We thank the National Institutes of Health (GM050781 to A.S.B.) for financial support. We thank Justin Lee for experimental assistance.

Notes and references

1. O'Brien JR, Schuller DJ, Yang VS, Dillard BD and Lanzilotta WN, Biochemistry, 2003, 42, 5547–5554. [PubMed: 12741810]
2. Vojtěchovský J, Chu K, Berendzen J, Sweet RM. and Schlichting I, Biophys. J, 1999, 77, 2153–2174. [PubMed: 10512835]
3. Gordon Z, Drummond MJ, Matson EM, Bogart JA, Schelter EJ, Lord RL and Fout AR, Inorg. Chem, 2017, 56, 4852–4863. [PubMed: 28394119]
4. Moore CM and Szymczak NK, Chem. Sci, 2015, 6, 3373–3377. [PubMed: 28706701]
5. Jones JR, Ziller JW and Borovik AS, Inorg. Chem, 2017, 56, 1112–1120. [PubMed: 28094522]
6. Cook SA and Borovik AS, Acc. Chem. Res, 2015, 48, 2407–2414. [PubMed: 26181849]
7. Shook RL and Borovik AS, Inorg. Chem, 2010, 49, 3646–3660. [PubMed: 20380466]
8. Borovik AS, Acc. Chem. Res, 2005, 38, 54–61. [PubMed: 15654737]

9. MacBeth CE, Gupta R, Mitchell-Koch KR, Young VG, Lushington GH, Thompson WH, Hendrich MP and Borovik AS, J. Am. Chem. Soc, 2004, 126, 2556–2567. [PubMed: 14982465]
10. Schwarz AD, Herbert KR, Paniagua C and Mountford P, Organometallics, 2010, 29, 4171–4188.
11. Schwarz AD, Chu Z and Mountford P, Organometallics, 2010, 29, 1246–1260.
12. Park YJ, Ziller JW and Borovik AS, J. Am. Chem. Soc, 2011, 133, 9258–9261. [PubMed: 21595481]
13. Park YJ, Cook SA, Sickerman NS, Sano Y, Ziller JW and Borovik AS, Chem. Sci, 2013, 4, 717–726. [PubMed: 24058726]
14. Cook SA, Ziller JW and Borovik AS, Inorg. Chem, 2014, 53, 11029–11035. [PubMed: 25264932]
15. Oswald VF, Lee JL, Biswas S, Weitz AC, Mittra K, Fan R, Li J, Zhao J, Hu MY, Alp EE, Bominaar EL, Guo Y, Green MT, Hendrich MP and Borovik AS, J. Am. Chem. Soc, 2020, 142, 11804–11817. [PubMed: 32489096]
16. Olmstead MM, Sigel G, Hope H, Xu X and Power PP, J. Am. Chem. Soc, 1985, 107, 8087–8091.
17. Chetcuti PA, Liégard A, Rihs G, Rist G and Schweiger A, Helv. Chim. Acta, 1991, 74, 1591–1599.
18. Sellmann D, Soglowek W, Knoch F, Ritter G and Dengler J, Inorg. Chem, 1992, 31, 3711–3717.
19. Fox DJ and Bergman RG, J. Am. Chem. Soc, 2003, 125, 8984–8985. [PubMed: 15369333]
20. Bowman AC, Bart SC, Heinemann FW, Meyer K and Chirik PJ, Inorg. Chem, 2009, 48, 5587–5589. [PubMed: 19361163]
21. Lee Y, Mankad NP and Peters JC, Nat Chem, 2010, 2, 558–565. [PubMed: 20571574]
22. Yu Y, Brennessel WW and Holland PL, Organometallics, 2007, 26, 3217–3226. [PubMed: 18725998]
23. Saouma CT, Moore CE, Rheingold AL and Peters JC, Inorg. Chem, 2011, 50, 11285–11287. [PubMed: 22004139]
24. Sickerman NS, Peterson SM, Ziller JW and Borovik AS, Chem. Commun, 2014, 50, 2515.
25. Harman WH and Chang CJ, 2007, 129, 15128–15129.
26. Ray M, Golombek AP, Hendrich MP, Young VG and Borovik AS, J. Am. Chem. Soc, 1996, 118, 6084–6085.
27. Weintrob EC, Tofan D and Bercaw JE, Inorg. Chem, 2009, 48, 3808–3813. [PubMed: 19301916]
28. Rittle J and Peters JC, Proc. Natl. Acad. Sci. U. S. A, 2013, 110, 15898–15903. [PubMed: 24043796]
29. Spasyuk DM, Carpenter SH, Kefalidis CE, Piers WE, Neidig ML and Maron L, Chem. Sci, 2016, 7, 5939–5944. [PubMed: 30034736]
30. lovan DA and Betley TA, J. Am. Chem. Soc, 2016, 138, 1983–1993. [PubMed: 26788747]
31. Eckert NA, Smith JM, Lachicotte RJ and Holland PL, Inorg. Chem, 2004, 43, 3306–3321. [PubMed: 15132641]
32. Nieto I, Ding F, Bontchev RP, Wang H and Smith JM, J. Am. Chem. Soc, 2008, 130, 2716–2717. [PubMed: 18266366]
33. Lucas RL, Powell DR and Borovik AS, J. Am. Chem. Soc, 2005, 127, 11596–11597. [PubMed: 16104724]
34. Saouma CT, Muller P, Peters JC, Muller P and Peters JC, J. Am. Chem. Soc, 2009, 131, 10358–10359. [PubMed: 19722612]
35. Leeladee P, Jameson GNL, Siegler MA, Kumar D, DeVisser SP and Goldberg DP, Inorg. Chem, 2013, 52, 4668–4682. [PubMed: 23527920]
36. Klinker EJ, Jackson TA, Jensen MP, Stubna A, Juhasz G, Bominaar EL, Muenck E and Que LJ, 2006, 45, 7394–7397.
37. Wilding MJT, Lovan DA and Betley TA, J. Am. Chem. Soc, 2017, 139, 12043–12049. [PubMed: 28777558]
38. Verma AK, Nazif TN, Achim C and Lee SC, 2000, 11013–11014.
39. Rhoda RN and Fraioli AV, 1953, 4, 159–161.
40. Connelly NG and Geiger WE, Chem. Rev, 1996, 96, 877–910. [PubMed: 11848774]
41. Evans DFJ. Chem. Soc1959, 2003–2005.

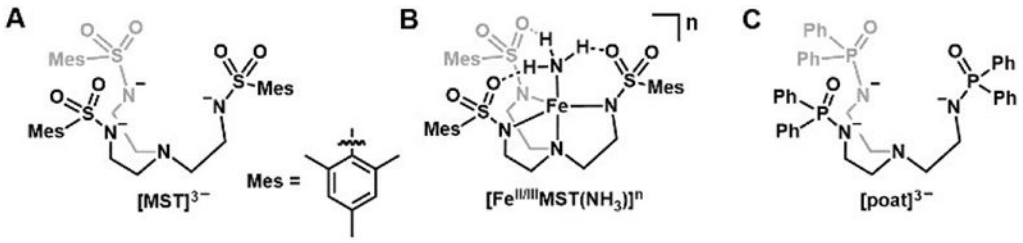

Figure 1.
Diagram of $[MST]^{3-}$ (A), $[Fe^{II/III}MST(NH_3)]^{-/0}$ complexes (B), and $[poat]^{3-}$ (C).

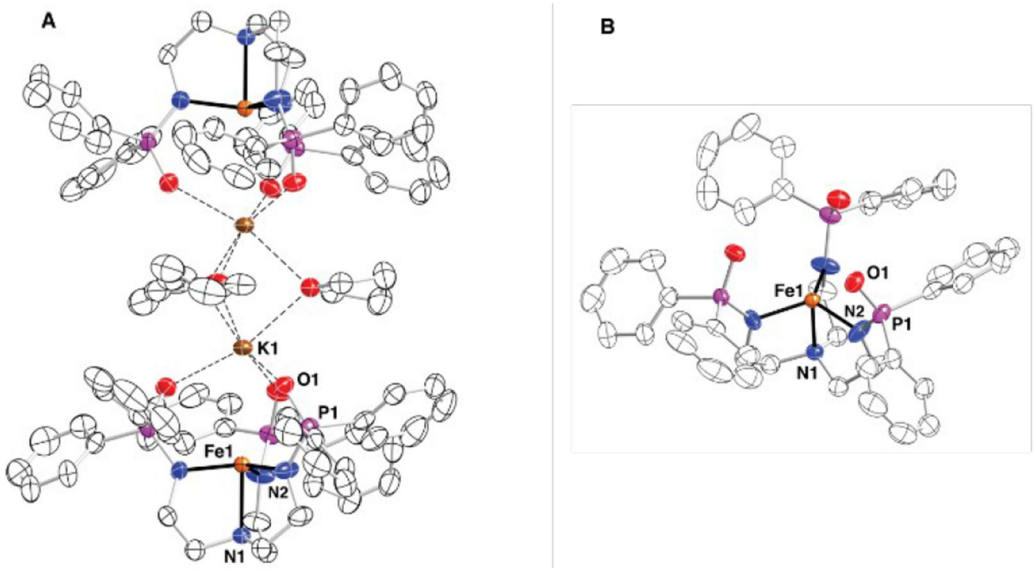

Figure 2.

Thermal ellipsoid plots of $\{K[Fe^{II}poat]\}_2 \cdot 3THF$ (A) and view of a $[Fe^{II}poat]^-$ fragment (B) determined by XRD methods. Hydrogen atoms are omitted for clarity and ellipsoids are drawn at the 50% probability.

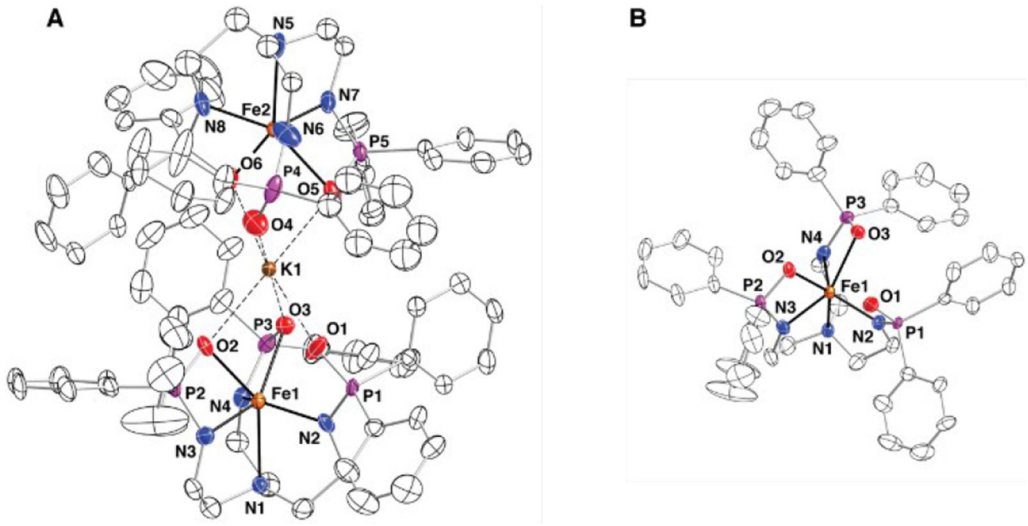

Figure 3.

Depiction of $\{K[Fe^{III}poat]_2\}^+$ (A) and view highlighting the $[Fe^{III}poat]$ fragment (B) determined by XRD methods. Hydrogen atoms and the $[BF_4]^-$ counter ion are omitted for clarity. Only one orientation of the disordered components is shown.

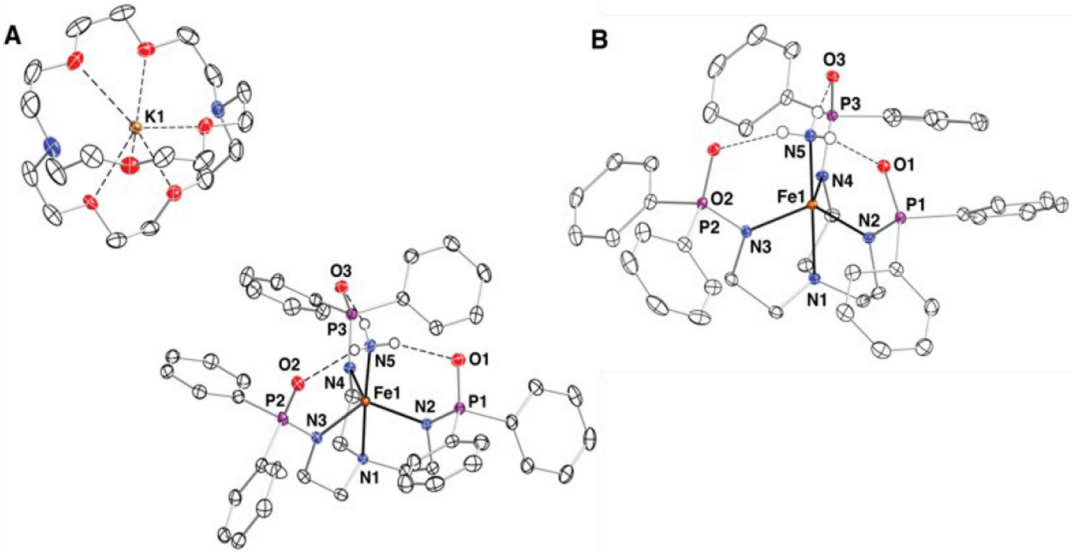

Figure 4.

Thermal ellipsoid plots of K(crypt)[Fe^{II}poat(NH_3)] (A) and [Fe^{III}poat(NH_3)] (B) determined by XRD methods. Only hydrogen atoms on NH_3 are shown; solvent molecules are omitted for clarity. Ellipsoids are drawn at the 50% probability.

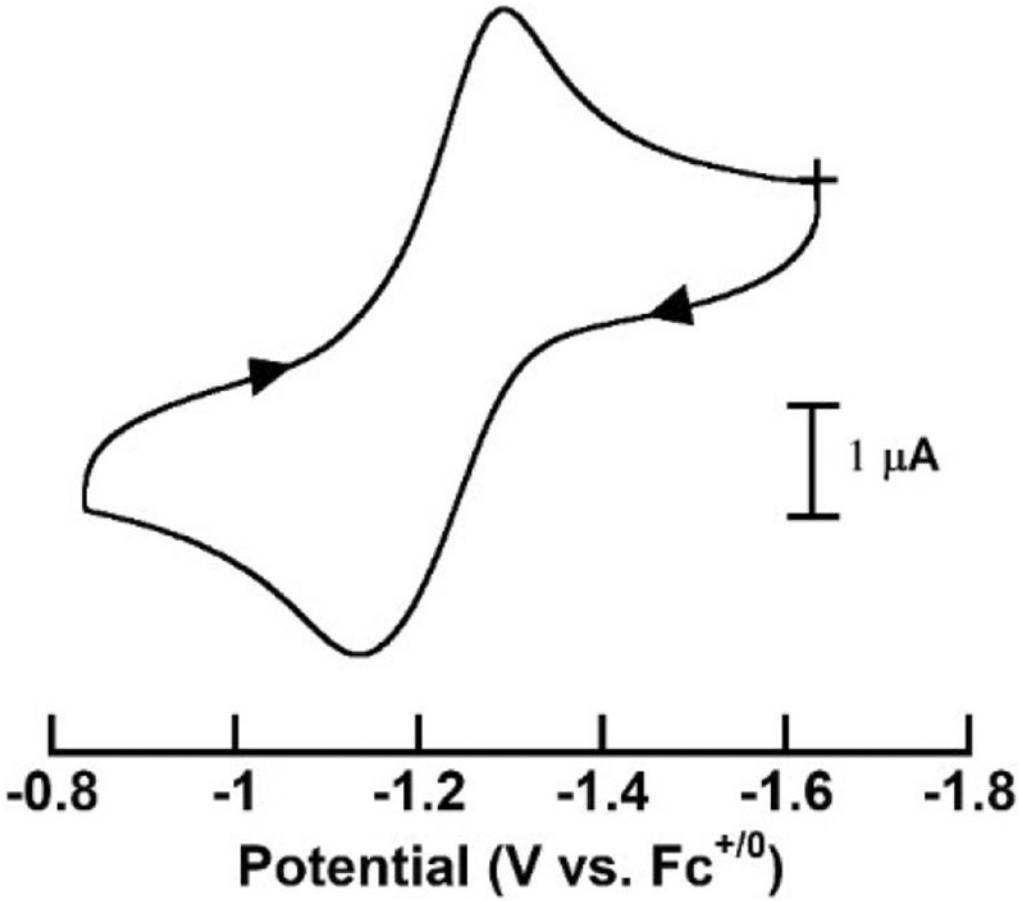

Figure 5.

CV of K(crypt)[Fe^{II}poat(NH_3)] in DCM:THF. The measurement was done with 100 mV/s scan rate using 100 mM tetrabutylammonium hexafluorophosphate ($TBAPF_6$) as electrolyte, glassy carbon electrode as working electrode, platinum wire as counter electrode, silver wire as reference electrode, and $[Fe^{III/II}Cp_2]^{+/0}$ couple as internal standard.

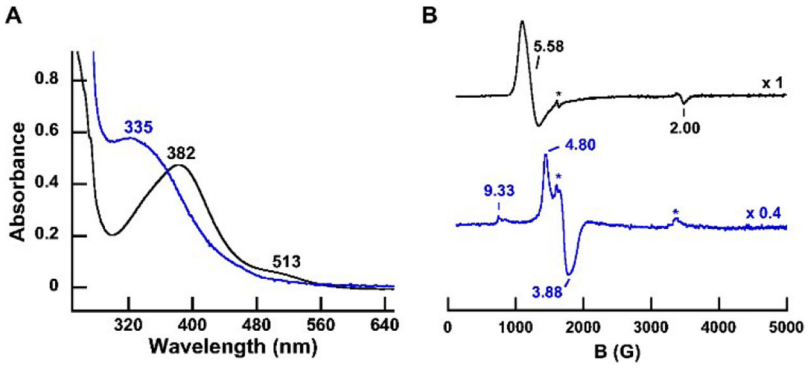

Figure 6.

(A) Electronic absorption spectra of before (black) and after (blue) addition of excess TBD to 0.13 mM [Fe^{III}poat(NH_3)] (black) in DCM. (B) EPR spectra of before (black) and after (blue) adding TBD to [Fe^{III}poat(NH_3)] in DCM:TFIF (⊥-mode, 77 K, 13 mM). Asterisks in panel B indicate signals from small amounts of impurities.

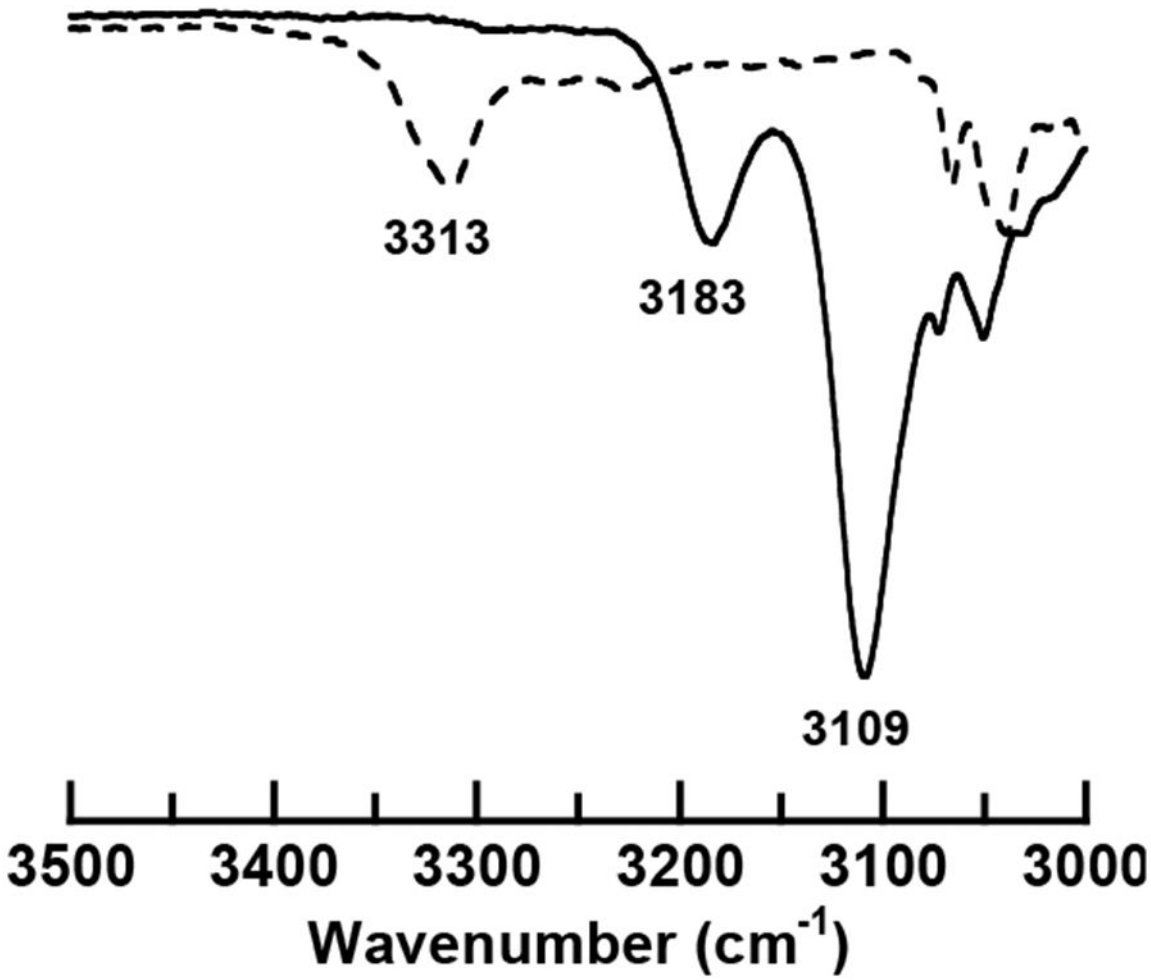

Figure 7.
Solid state FT-IR spectra of K(crypt)[Fe^{II}poat(NH_3)] (dash line), and [Fe^{III}poat(NH_3)] (solid line).

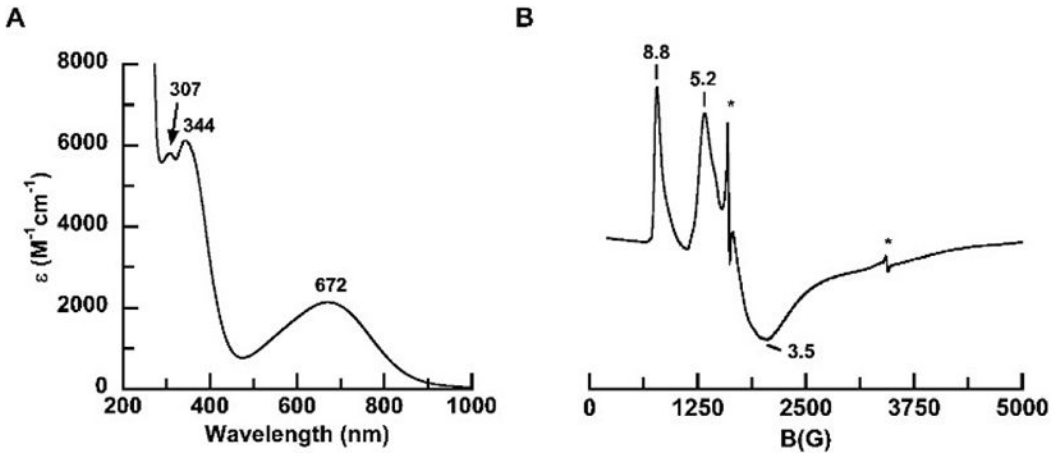

Figure 8.

Electronic absorption spectrum (A) and EPR spectrum (⊥-mode, 3.9 K) (B) of K[Fe^{III}poat(NHtol)] in DMF:THF. Asterisks in panel B indicate signals from small amounts of impurities.

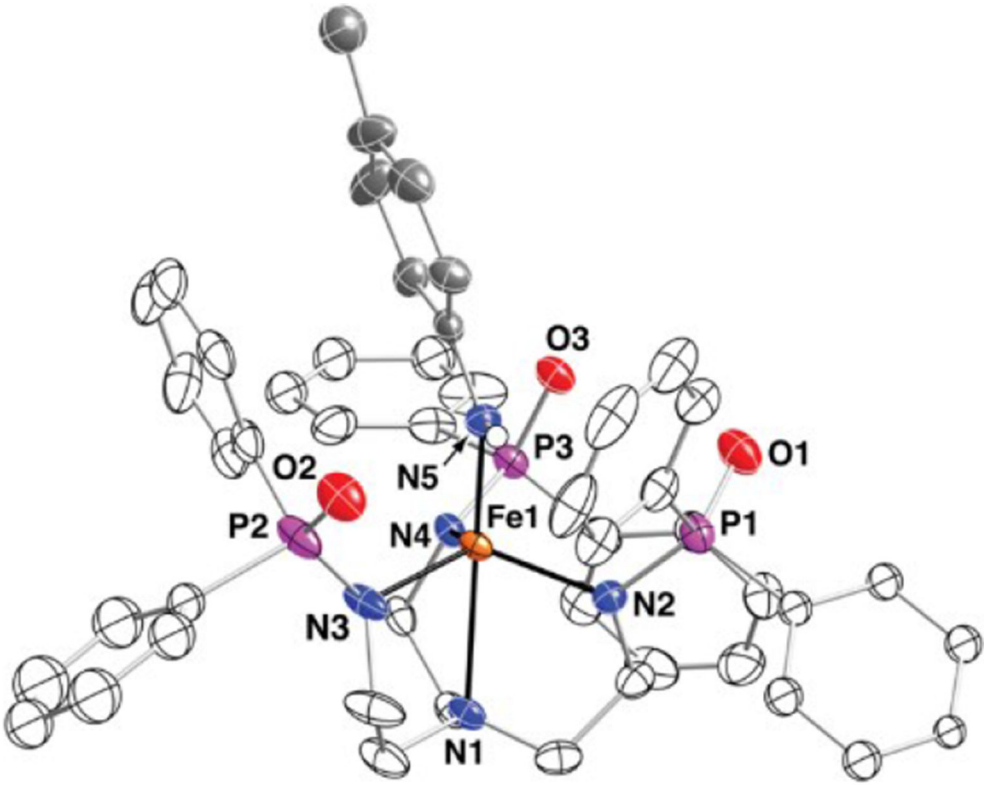

Figure 9.

Thermal ellipsoid plots of $[Fe^{III}poat(NHtol)]^{-}$ determined by XRD methods. Only the hydrogen atom on amido ligand is shown. Carbon atoms on the amido ligand are highlighted in grey to distinguish from the other carbon atoms. Ellipsoids are drawn at the 50% probability. Only one orientation of the disordered molecule is shown.

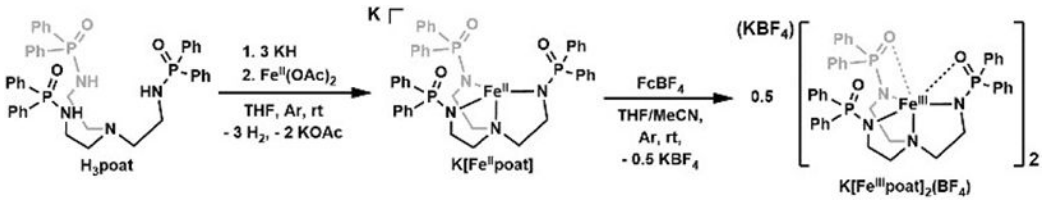

Scheme 1.

Synthesis of $\{K[Fe^{II}poat]\}_2$ and $\{K[Fe^{III}poat]_2\}^+$.

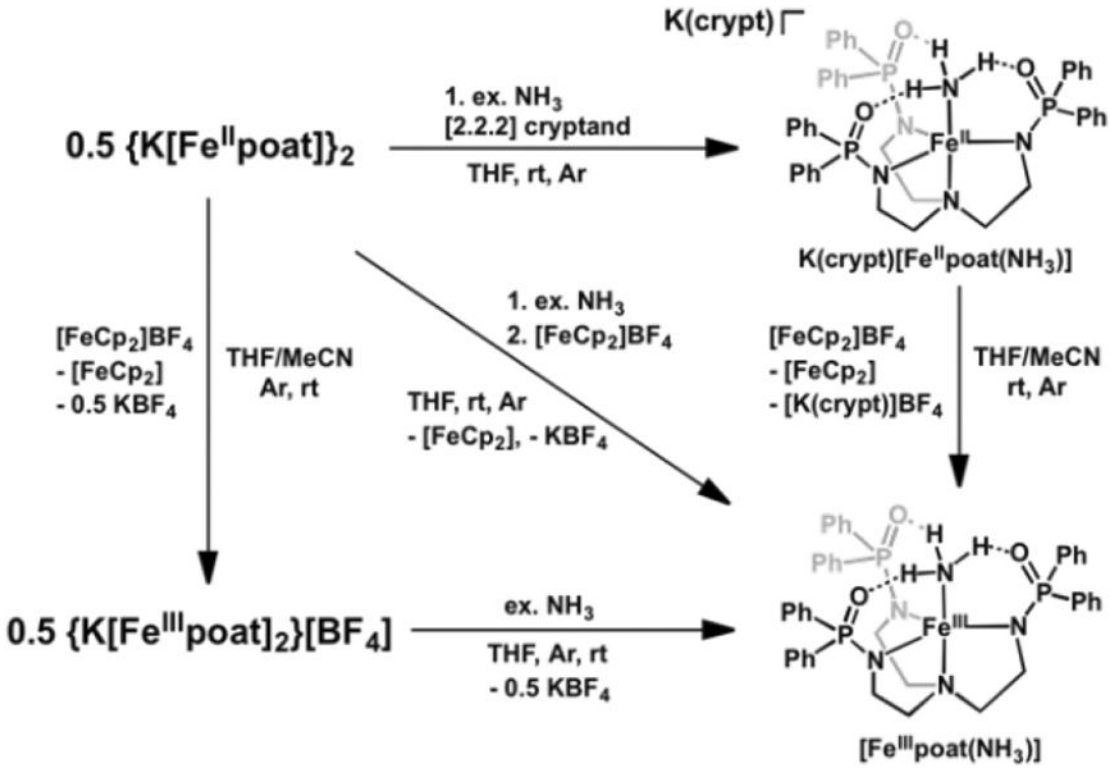

Scheme 2.
Synthesis of K(crypt)[Fe^{II}poat(NH_3)] and [Fe^{III}poat(NH_3)].

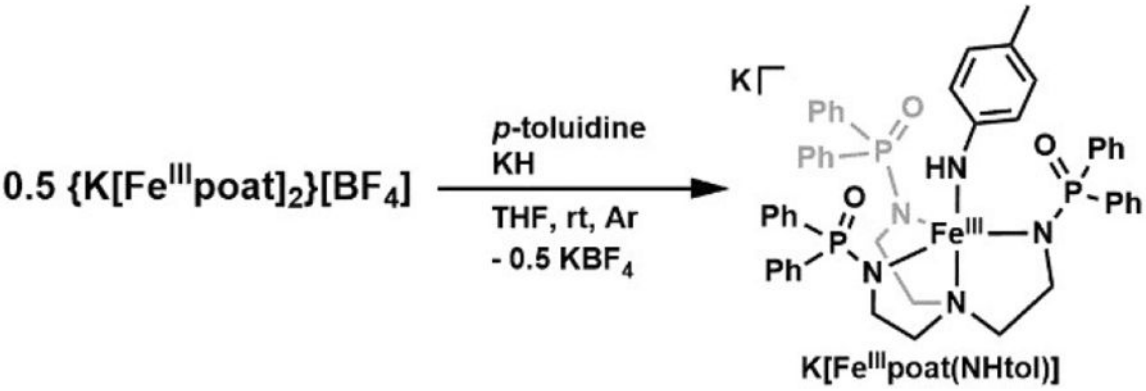

Scheme 3.
Synthesis of K[Fe^{III}poat(NHtol)].

Table 1.

Selected bond lengths (Å) and angles (°) for $\{K[Fe^{II}poat]\}_2 \cdot 3THF$ and $\{K[Fe^{III}poat]_2\}^+$

Complex	$\{K[Fe^{II}poat]\}_2 \cdot 3THF$	$\{K[Fe^{III}poat]_2\}^+$
	Bond Distances (Å)	
Fe1—N1	2.127(4)	2.336(5)
Fe1—N2	1.994(2)	1.972(5)
Fe1—N3	-	1.999(5)
Fe1—N4	-	2.004(5)
Fe1—O2	-	2.235(5)
Fe1—O3		2.323(4)
	Bond Angles (°)	
N1—Fe1—N2	83.62(7)	78.0(2)
N1—Fe1—N3	-	78.2(2)
N1—Fe1—N4	-	75.1(2)

Table 2.

Selected distances (Å) and angles (°) for $[Fe^{II/III}poat(NH_3)]^{-/0}$ and $[Fe^{III}poat(NHtol)]^{-}$ and related Fe complexes with $[MST]^{3-}$ for comparison.

Complexes	K(crypt)[$Fe^{II}poat(NH_3)$]	[$Fe^{III}poat(NH_3)$]^a	Na[$Fe^{II}MST(NH_3)$]^b	[$Fe^{III}MST(NH_3)$]^b	K[$Fe^{III}poat(NHtol)$]
			Distances (Å)		
Fe1—N1	2.220(1)	2.220 (4)	2.224(1)	2.295(3)	2.401(3)
Fe1—N2	2.112(1)	1.998(3)	2.096(1)	1.979(2)	2.030(3)
Fe1—N3	2.110(1)	-	2.098(1)	-	2.004(3)
Fe1—N4	2.104(1)	-	2.104(1)	-	2.040(3)
Fe1—N5	2.143(2)	2.060(4)	2.145(1)	2.080(3)	1.950(3)
N5…O1	2.884(2)	2.774(3)	2.810(2)	2.881(2)	-
N5…O2	2.921(2)	-	2.914(2)	-	-
N5…O3	2.988(2)	-	2.918(2)	-	-
			Angles (°)		
N1—Fe1—N5	177.74(6)	180.0	177.58(5)	180.0	168.79(12)

^{a}bond lengths and angles are reported as an average

^{b}from ref 24.